Nanoscale

Accepted Manuscript

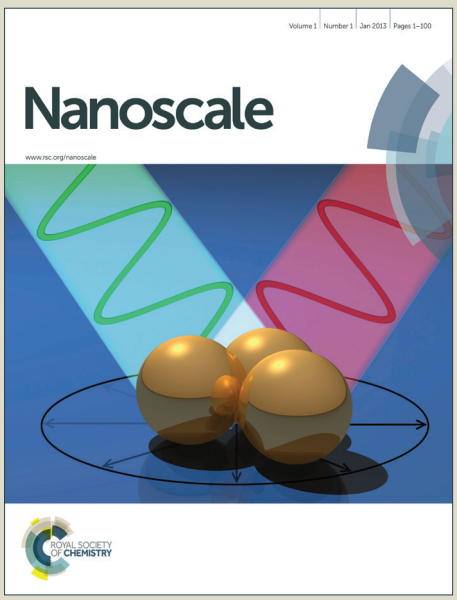

ROYAL SOCIETY OF CHEMISTRY

www.rsc.org/nanoscale

Cite this: DOI: 10.1039/c0xx00000x

www.rsc.org/xxxxxx

ARTICLE TYPE

Graphene field effect transistor as a probe of electronic structure and charge transfer at organic molecule-graphene interfaces

Jiri Cervenka,*[a] Akin Budi,[#a] Nikolai Dontschuk,[a] Alastair Stacey,[a] Anton Tadich,[b,c] Kevin J. Rietwyk,[$c] Alex Schenk,[c] Mark T. Edmonds,[c,d] Yuefeng Yin,[e] Nikhil Medhekar,[e] Martin Kalbac[f] and Chris I. Pakes[c]

Received (in XXX, XXX) Xth XXXXXXXXX 20XX, Accepted Xth XXXXXXXXX 20XX
DOI: 10.1039/b000000x

The electronic structure of physisorbed molecules containing aromatic nitrogen heterocycles (triazine and melamine) on graphene is studied using a combination of electronic transport, X-ray photoemission spectroscopy and density functional theory calculations. The interfacial electronic structure and charge transfer of weakly coupled molecules on graphene is found to be governed by work function differences, molecular dipole moments and polarization effects. We demonstrate that molecular depolarization plays a significant role in these charge transfer mechanisms even at submonolayer coverage, particularly for molecules which possess strong dipoles. Electronic transport measurements show a reduction of graphene conductivity and charge carrier mobility upon the adsorption of the physisorbed molecules. This effect is attributed to the formation of additional electron scattering sites in graphene by the molecules and local molecular electric fields. Our results show that adsorbed molecules containing polar functional groups on graphene exhibit different coverage behaviour to nonpolar molecules. These effects open up a range of new opportunities for recognition of different molecules on graphene-based sensor devices.

Introduction

Understanding and controlling the fundamental electronic processes at the interfaces between conjugated organic molecules and electrically conductive surfaces is of considerable interest for many important technological applications, including organic electronics, solar cells and sensors.[1–3] Although the interfacial electronic structure of metal-organic systems has been the subject of intense research for a long time,[4,5] the rich interplay of physics, diversity of molecular structures and the importance of weak and long range interactions has made the understanding of these interface electronic structures difficult. The use of a two dimensional (2D) substrate can provide new insights into these problems by simplifying the role of the (typically 'bulk') metal substrate. Additionally, the use of conductive 2D materials opens up entirely new opportunities, providing access to information about the molecular-substrate interactions through electronic transport measurements and potential for developing new sensor devices.

Graphene, a single layer of graphite, is an ideal 2D material for probing these interfacial molecular-substrate interactions because of its extraordinary electrical, optical, thermal, and mechanical properties.[6,7] Graphene is a semimetal and its majority charge carriers can be tuned from electrons to holes by an external electric field.[8] This allows precise determination of the charge neutrality point (Dirac point) and the doping type in graphene field effect transistors (FETs).[9] Moreover, recent studies have shown that the electronic structure of graphene can be effectively tuned between *n*-type or *p*-type doping by the adsorption of various electron donating/accepting molecules.[10–12] A combination of these mechanisms provides a unique tool for studying and detecting different gases, organic molecules, biomolecules and other substances. Previous reports have demonstrated this sensing ability of graphene, showing extreme sensitivity to the adsorption of different molecules,[13–15] and even achieving a single-molecule detection limit with NO_2.[13] Such high sensitivity can be explained by the extremely low electronic noise characteristics and high specific surface area of graphene.[16–18] Although graphene sensors have proven to be highly sensitive, their ability to distinguish between different molecular species (selectivity) remains a major problem for practical applications. Another major hurdle for graphene-based sensors is the detection of weakly interacting organic molecules and molecular recognition of non-covalent interactions. A good understanding of these effects and their limitations is essential for the advancement of graphene chemical sensors and hybrid organic-graphene nanoelectronics.

Here we present a combined experimental and theoretical study of small organic molecules adsorbed on CVD graphene and investigate their role in the modification of the graphene electronic structure. We use graphene FETs to sense molecular adsorption processes occurring on their surfaces via changes in the chemical potential of graphene. In particular, we focus on two similar organic molecules containing aromatic nitrogen heterocycles, 1,3,5 triazine and melamine, and investigate how different chemical functional groups manifest in electronic transport measurements for selective chemical sensing. We investigate the mechanism of charge transfer doping and the

existence of molecule specific signatures in FET electrical conductivity measurements and compare these results with synchrotron-based X-ray photoelectron spectroscopy (XPS) measurements and density functional theory (DFT) calculations. We demonstrate that graphene-based FETs are a sensitive and versatile tool for studying the interfacial electronic structure, charge transfer processes and collective molecular electric fields of weakly coupled molecules on graphene.

Experimental

The graphene samples used in this study were grown by chemical vapor deposition (CVD) on Cu foils and transferred onto SiO_2 (90 nm) / *n*-Si(100) substrates using a polymethyl methacrylate (PMMA) transfer method.[19,20] The thickness of the graphene layer across each sample was confirmed to be 1 monolayer (ML) using Raman spectroscopy.[†] The samples were annealed at 270 °C in Ar atmosphere for a few days to improve their surface cleanliness. Each graphene sample was divided into two adjacent areas to allow for simultaneous electric and XPS characterization at each molecular coverage. For the electronic measurements, Ti/Au (10/100 nm) contacts with 50 μm separation were deposited onto the graphene using e-beam evaporation through a shadow mask. The graphene was patterned using PMMA protective layers followed by O_2 plasma etching. The samples were then introduced into a vacuum chamber and annealed at 250-300 °C for at least 2 h in order to remove water and other airborne contamination. Deposition of triazine and melamine was performed using a low temperature effusion cell (MBE Komponenten GmbH) operating at 140 and 175 °C, respectively. Increasing melamine coverage was achieved by incremental molecular depositions on graphene at room temperature between each XPS and electronic measurement. Since triazine desorbs from graphene at room temperature, we controlled the molecular coverage of triazine by depositing a thick layer at -100 ºC and performed the measurements while triazine slowly desorbed off the graphene surface. Both XPS and electronic transport measurements were conducted after each deposition, on the two separate pieces of each graphene sample respectively, in an ultra-high vacuum (UHV) chamber at the Soft X-ray beamline at the Australian Synchrotron. To avoid possible beam damage of the molecules, different measurement positions were used for each XPS scan. All experiments, including deposition of molecules, were carried out under UHV conditions with pressures below 1×10^{-9} mbar to avoid any interference from air or water contamination during the measurements. Pressures higher than 1×10^{-8} mbar have been observed to cause a small shift in the chemical potential of graphene, which would interfere with the measured signals from the deposited molecules.

Results and Discussion

Fig. 1 shows electronic transport measurements of a graphene FET device on SiO_2/Si as a function of gate voltage (V_G) for increasing melamine coverage. A schematic outline and optical profiler images of the corresponding single layer bottom-gated graphene FET are shown in Fig. 1(a-b). The device characteristics of pristine graphene (Fig. 1c) shows the typical ambipolar transport behaviour with a minimum source-drain current (I_{SD}) at -6.5 V, which is related to the difference between the charge neutrality point (the Dirac point) and the position of the Fermi level in graphene. The clean graphene is therefore slightly n-type doped, in accordance with previous reports.[21] The gate dependence of I_{SD} shows a clear change upon adsorption of the molecules onto the graphene FET, with the Dirac point shifting to the right (higher gate voltage) with deposition of melamine. This corresponds to electron removal (*p*-type doping) of the graphene by melamine. The FET thus serves as a chemical sensor, and reacts measurably to the interaction of graphene with a small number of molecules (10^3-10^5 per μm^2). Deposition of triazine on graphene FETs have resulted in a similar behaviour to melamine.[†] The observed reduction of the minimum conductivity in the FET spectra can be attributed to either a change in contact resistance or graphene-substrate interactions, due to adsorption of the molecules. Any contact resistance change can be qualitatively understood by a molecule-induced work function realignment of the metal electrodes.[22] The latter effect might arise from the interaction of adsorbed molecules with charge impurities in the SiO_2 substrate, which has been reported to induce electron-hole puddles in graphene.[23] The formation of these electron-hole puddles is also currently one of the most accepted mechanisms for broadening of the minimal conductivity region in graphene FET measurements.[24,25]

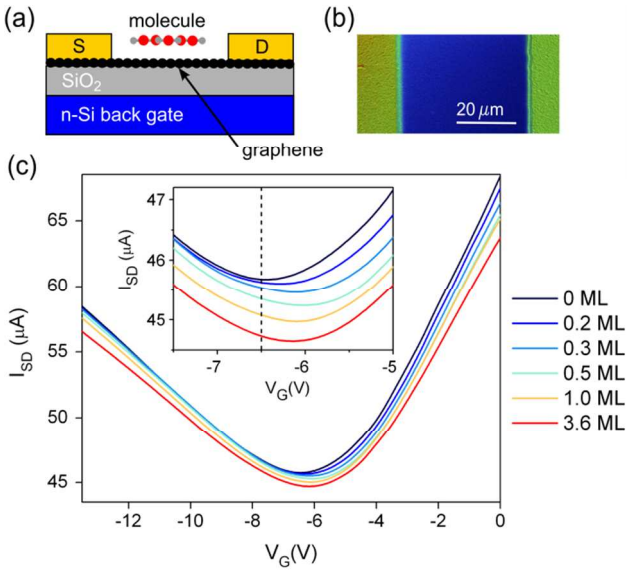

Fig 1. (a) Schematic illustration of the cross-section through a graphene FET with adsorbed molecules on the surface. (b) An optical profiler map of the top surface of a graphene channel and Ti/Au electrodes in FET devices. (c) Gate voltage dependent source-drain current (I_{SD}) spectra of a graphene FET at a constant source voltage (V_{SD} = 50 mV) as a function of increasing melamine coverage. The inset shows a positive shift of the conductivity minimum (the Dirac point) upon adsorption of melamine, corresponding to *p*-type doping of graphene by melamine.

Utilizing the same graphene sample, we carried out a comparative study using synchrotron-based XPS measurements on the large flat graphene area neighbouring the FET structures. We measured XPS spectra of graphene using 330 eV photons and monitored the changes of the C1s peak of graphene as a function of increasing molecule coverage, as shown in Fig. 2. By

simultaneously monitoring the N1s spectra (using 500 eV photons for similar surface sensitivity) we could precisely determine the average molecular coverage deposited on the graphene surface. This was achieved by comparing the N1s peak area to the C1s peak area of monolayer graphene, taking the advantage of the similar kinetic energy of photoelectrons and correcting for their respective photoionization cross sections.[†]

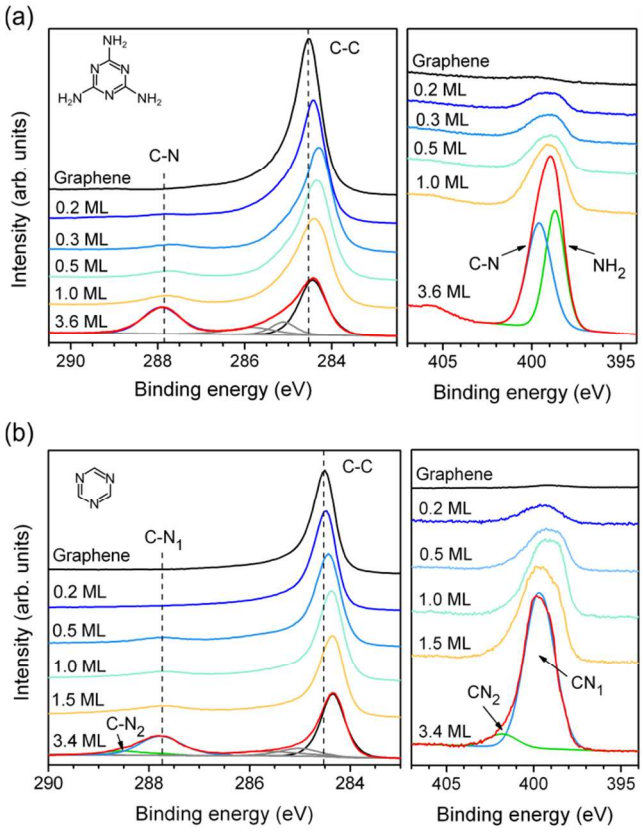

Fig 2. XPS C1s ($h\nu$ = 330 eV) and N1s ($h\nu$ = 500 eV) spectra of graphene with increasing coverages of (a) melamine and (b) triazine.

The C1s core-level spectrum of graphene with triazine and melamine contains two groups of peaks, as shown in Fig. 2. The group at 284.5 eV corresponds to CVD graphene, and the second group around 288 eV represents the C-N bonds in triazine and melamine. The tail C-N_2 peak for the high triazine coverage data is attributed to electron charging on thicker molecular islands. It is clear that, aside from a binding energy shift, the lineshape of the graphene C1s remains unchanged with the addition of the molecular adlayers, indicating no chemical bonding of these molecules with the substrate. Due to the large energy separation of the molecular and graphene peaks, we can use the position of the graphene C1s peak as a probe of the electronic structure modification of graphene induced by the molecules. The C1s peak position of graphene can be used as a measure of the shift in the chemical potential (doping) of graphene. There is a clear downwards shift in binding energy of the C1s peak of graphene for both molecules upon molecular deposition, corresponding to an increase of the chemical potential of graphene due to either direct electron transfer from graphene to the molecules or other indirect electron rearrangement processes. The XPS data therefore shows qualitative agreement with the FET results. It is important to note here that the position of the graphene C1s peak fully recovered to its initial position after completely removing the deposited molecules with a short anneal of the substrates at 200 ºC. This result again confirms that both triazine and melamine are weakly bound to graphene, and furthermore that the electronic structure of graphene recovers upon desorption of these molecules from the surface.

One of the main advantages of the FET-based measurements, when compared with XPS methods, is that they provide better sensitivity of the molecule-induced signals in graphene. While the measured shifts in XPS peak position are very close to the energy resolution limit (~0.05 eV) of the synchrotron XPS system, the FET measurement precision is essentially limited by electronic noise in our electronic devices (10^{-7} A and 1 mV). Moreover, the determination of the charge neutrality point in our FET measurements can be even further improved by using higher mobility graphene with steeper I_{DS}-V_G characteristics, such as reported in recent studies of graphene on BN.[26,27]

In Fig. 3, we compare the electronic transport and XPS data as a function of molecular coverage of triazine and melamine on graphene. The electrical data represents the induced charge carrier density (Δn) of graphene caused by the molecules. The Δn values have been obtained by using the observed voltage shifts of the conductivity minima in graphene with the known back gate capacitance of the SiO_2 dielectric layer (C_G = 3.84×10^{-4} Fm^{-2}) according to the following expression $n = C_G V_{min}/e$.[28] The XPS results are plotted as shifts in binding energy of the C1s peak of graphene, *i.e.* changes of the chemical potential. Overall, there is a very good correspondence between the XPS and FET data, which clearly shows that the measured changes originate from the same mechanism. Additionally, it confirms that the measured FET signals are caused predominantly by the graphene-molecule interactions and not by molecular interactions with the metal contacts.

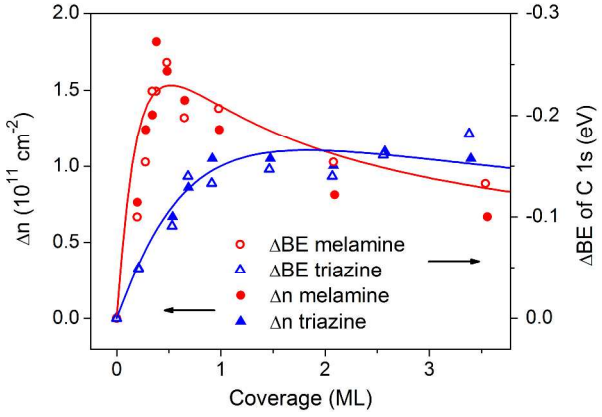

Fig 3. A comparison between triazine and melamine coverage dependence of change in graphene carrier density (full symbols) determined from the shift of the charge neutrality point in electronic transport measurements and binding energy shifts (ΔBE) of the C1s peak of graphene (open symbols) determined from XPS. The solid lines represent fits to the ΔBE data points using an electrostatic depolarization model (Eq. 3).

Interestingly, the coverage profiles differ significantly for melamine and triazine. While we observe a saturating molecular coverage dependence for triazine with a maximum shift at about a monolayer, the situation is quite different for melamine. The

melamine data show a maximum shift at coverage of about 0.4 ML followed by a slow decay at higher coverages. This behaviour is a typical signature of depolarization effects in the adsorbed molecular layers.[29] Similar results have been previously observed in coverage-dependent work function measurements of transition metals and organic molecules on metal substrates,[29–33] and recently also in density functional theory (DFT) calculations of Li on graphene.[34] To check that the observed effect is not a result of structural changes in the molecular layer, we have performed angle dependent NEXAFS measurements to determine the orientation of the molecules on the graphene surface.[†] As expected from previous studies of triazines on graphene and graphite,[35,36] both molecules adsorb on graphene in a flat geometry and we did not find any significant change in their arrangement with increasing coverage.

Fig. 4 shows a change of charge carrier mobility of graphene as a function of triazine and melamine coverage. The graphene charge carrier mobility was derived using constant mobility model,[28,37] where the mobility (μ) was obtained from linear fits of the electron and hole branches of the I_{DS}-V_G characteristics using $\Delta I_{DS}/\Delta V_G = ne\mu$. Due to the initial asymmetry between the hole and electron conduction regimes in the clean graphene device on SiO_2,[38] the hole mobility is found approximately twice as large as the electron mobility. The adsorption of the molecules gives rise to a further increase in this asymmetry, exhibiting a larger change of the slope in the hole conductivity region (Fig. 1). Overall, the mobility of the graphene FETs decreases with increasing molecule coverage. Melamine data shows the maximum mobility at 0.3 ML, which is the molecular coverage inducing the largest charge neutrality point shift in graphene (Fig. 3). The triazine data shows saturation of both electron and hole mobility above 1 ML coverage, which is in line with the coverage dependence of molecule induced charge carrier density in graphene in Fig. 3.

The decrease of graphene conductivity and mobility with increasing molecule coverage can be explained by three possible effects. The first one is related to a change of the dielectric environment by adsorption of the molecules on the graphene surface. Newaz *et al.* have reported that graphene devices immersed in polar liquids demonstrate much lower mobility than devices immersed in nonpolar liquids.[37] This trend has been explained by different dielectric screening of charged impurities in graphene and the SiO_2 substrate.[37] The higher polarity of melamine in respect to triazine could possible explain the larger reduction of graphene mobility with melamine (12% reduction of hole mobility) than triazine (5% reduction of hole mobility). The second possible effect explaining the flattening and the increased asymmetry in I_{DS}-V_G measurements is related to a molecular-induced change in the interfacial potential barrier at the metal-graphene contacts.[39,40] The metal-graphene interface barrier has been found to significantly limit the charge transport and carrier tunnelling probability in the FET devices.[40] The role of the molecules on the contact resistance, however, could not be explored in two terminal devices used in this study. The third option is that the molecules act as direct scattering sites in graphene transport by inducing additional local electric fields in graphene, which results in a reduction of graphene mobility.[28,37] A formation of such molecule-induced electric fields is explained later in the text using density functional theory calculations.

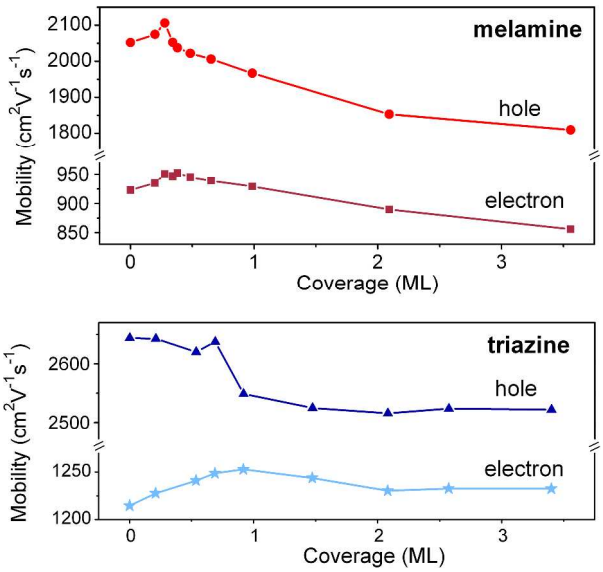

Fig 4. Graphene charge carrier mobility as a function of increasing melamine (top) and triazine (bottom) coverage. The charge carrier mobility was determined from the linear fits of I_{DS}-V_G characteristics.

To explain the different coverage characteristics of melamine and triazine on graphene, we use a simple electrostatic depolarization model to derive the chemical potential modification in graphene induced by the adsorption of a thin film of dipolar molecules.[29,41] The system is described as the charging of a parallel plate capacitor of molecular length with the far-field established outside of the top plate. Each molecule possesses a dipole moment ($\boldsymbol{\mu}$) that generates an electric field at distance $\mathbf{r}$ as

$$\mathbf{E}(\mathbf{r}) = \frac{1}{4\pi\varepsilon_0}\left(\frac{3(\boldsymbol{\mu}\cdot\mathbf{r})\mathbf{r} - \boldsymbol{\mu}}{r^3}\right). \quad (1)$$

Restraining the problem to only the z-direction (perpendicular to the graphene plane), this field polarizes neighbouring molecules in the adlayer, giving rise to a net dipole moment

$$\mu_z = \mu_{0z} + \alpha E_z, \quad (2)$$

where α is the polarizability of the molecules and μ_{0z} is the point dipole moment associated with each molecule. The energy change of the chemical potential upon physisorption of polar molecules is akin to establishing a potential difference by charging the molecular plate capacitor. The potential can be calculated by performing the lattice summation of the electric field from all oriented dipole moments in the adlayer as[29]

$$\Delta E = e\Delta V = \frac{e\mu_{0z}N}{\varepsilon_0(1 + c\alpha N^{3/2})}, \quad (3)$$

where N is the number of surface-coating adsorbates per unit area and $c \approx 10$, a geometric factor resulting from an infinite grid structure summation.[32] Fits to the XPS experimental data using Eq. (3) with two fit parameters (μ_{0z} and $c\alpha$) are shown by solid lines in Fig. 3 and the fit parameters are given in Tab. 1. The simple electrostatic depolarization model suggests that the coverage profile of melamine is a consequence of a strong molecular dipole moment, of the order of 0.5 eÅ. Although this

model does not include quantum mechanical effects, it describes the measured data very well. The validity of this model has previously been tested on different molecule-metal systems and it has been found that it models the interfacial interactions in good agreement with quantum mechanical calculations.[29]

To gain a more accurate theoretical insight in the observed effects, we also performed electronic structure calculations of the molecules on graphene using density functional theory (DFT) using the Vienna *ab-initio* simulation package (VASP).[42] We used the generalized gradient approximation (GGA) of Perdew-Burke-Ernzerhof (PBE) for the electron exchange-correlation functional[43] including van der Waals corrections, using a semiempirical functional developed by Grimme (DFT-D2).[44] The details of the DFT calculations are described in Supplemental Material.† Fig. 5 illustrates the optimised geometry and band structures of graphene upon adsorption of triazine and melamine on graphene. Both molecules are physisorbed on graphene with binding energies of -0.42 and -0.66 eV for isolated triazine and melamine molecules on the 7×7 graphene supercell respectively. The binding energy has been found to decrease slightly to -0.41 eV and -0.62 eV for higher molecular coverage using the 4×4 graphene supercell. The band structure of graphene shows that there is no hybridization of the frontier molecular orbitals with low energy π electrons of graphene. Additionally, there is no observable shift of the Dirac point of graphene upon adsorption of the molecules. The hybridized highest occupied and lowest unoccupied molecular orbitals with graphene are far from the Fermi level of graphene, as highlighted by the red lines in the band structures in Fig. 5. The DFT calculations therefore indicate overall weak interactions of the molecules with graphene via a predominance of dispersive forces.

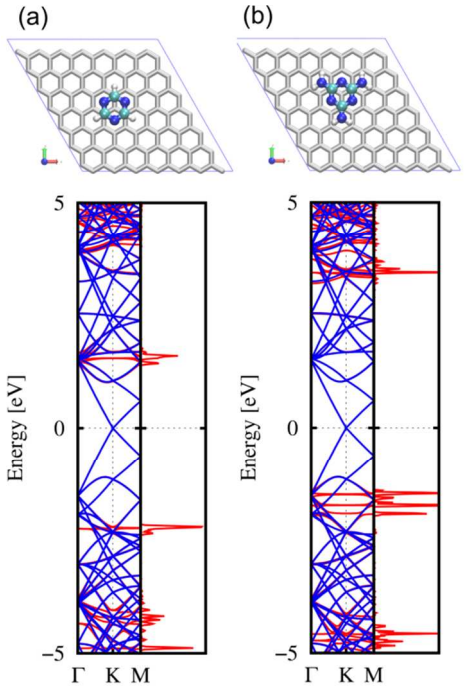

Fig 5. Optimized geometry and band structures of graphene with adsorbed (a) triazine and (b) melamine on the surface. The red lines in the band structures highlight the contributions of the hybridized molecular states in the electronic structure of graphene.

In the case of weak interactions, the interfacial molecule-graphene electronic structure is better described by calculating the work function difference between clean graphene and graphene with the adsorbed molecules. Tab. 1 summarizes the DFT calculated work function change ($\Delta\Phi$), charge transfer (Δq) between the molecules and graphene and electric dipole moments (μ_z) of triazine and melamine on graphene. There is only a small net charge transfer from graphene to the molecules, which scales up roughly with the adsorption energy. On the other hand, we can see that the work function of graphene significantly increases by 0.28 eV with the adsorption of melamine on graphene, a smaller change with triazine of the order of 0.05 eV. Although the trend of the calculated work function changes agree with the observed C1s shifts in the XPS data and FET measurements, the magnitude differs significantly. This shows that the measured signals result from a combination of different effects. Therefore, the resulting interface electronic structure is not only influenced by the work function change but also by direct charge transfer and charge redistribution within the molecule-graphene system.

Tab 1. Calculated work function change ($\Delta\Phi$) and charge transfer (Δq) of graphene with the adsorbed molecules and electric dipole moments (μ_z) of triazine and melamine on graphene using DFT. The out-of-plane point dipole moment (μ_{0z}) of the molecular layers and polarizability parameters ($c\alpha$) determined from fitting XPS data using the electrostatic depolarization Eq. (3).

Molecule	$\Delta\Phi$ (eV)	Δq (e/ mol)	μ_z (e Å)	μ_{0z} fit (e Å)	$c\alpha$ fit (Å^3)
Triazine	0.046	0.055	0.010	0.061	0.65
Melamine	0.279	0.076	0.482	0.549	6.2

DFT calculations predict the formation of a strong dipole moment in the direction perpendicular to the graphene surface in the graphene-melamine complex (0.48 eÅ) and a negligible dipole moment for triazine on graphene (0.01 eÅ). The molecular dipole moments per a molecule have not been found to change between submonolayer (7×7 graphene supercell) and monolayer (4×4 graphene supercell) coverages. The calculated dipole moments (Tab. 1) using DFT calculations yield qualitative agreement with the out-of-plane point dipole moments (μ_{0z}) of the molecular layers determined from fitting the XPS data in Fig. 3 using the electrostatic depolarization model (Eq. 3). The interface dipole moments originate predominantly from charge separation within the adsorbed molecules. Fig. 6 shows how the charge rearrangement in the free molecules leads to a change in the electrostatic potential between the vacuum levels towards graphene and vacuum side of the order of 0.292 and 0.003 eV for melamine and triazine, respectively. By comparing the potential drop across the free molecules to the work function change of graphene shown in Tab. 1, we can clearly see that it is the molecular dipoles which play a dominant role in the energy level alignment in the molecule-graphene system. The molecular dipoles act as local sources of electric field, producing electrical inhomogeneities in graphene. These local molecular fields can be one of the possible explanations for the observed decrease in the mobility of graphene upon the adsorption of the molecules.

The resulting out-of-plane dipole moment of adsorbed melamine on graphene is further enhanced in the z-direction in comparison to the free molecules owing to a tilt of hydrogen

atoms in the amino groups by 25° towards graphene after adsorption (Fig. 6). Angle-resolved NEXAFS measurements of nitrogen K-edge support this theoretical prediction by measuring a tilt angle of about 8° for the N amino π* resonance in respect to the planar axis of the molecules.† Since both triazine and melamine have the same atomic structure, except for the additional amino groups in melamine, the measured difference between these two molecules can be attributed to the presence of the polar amino groups. This highlights the importance of polar functional groups on the interfacial molecule-graphene electronic structure modification. These effects can be exploited in recognition of different molecules on graphene sensors. However, care needs to be taken at the higher molecular coverages where depolarization effects can prevail, as shown for melamine. The mutual collective interaction between individual dipole moments can significantly suppress the total electric field from the molecular layers, leading to a small change of the chemical potential of graphene.

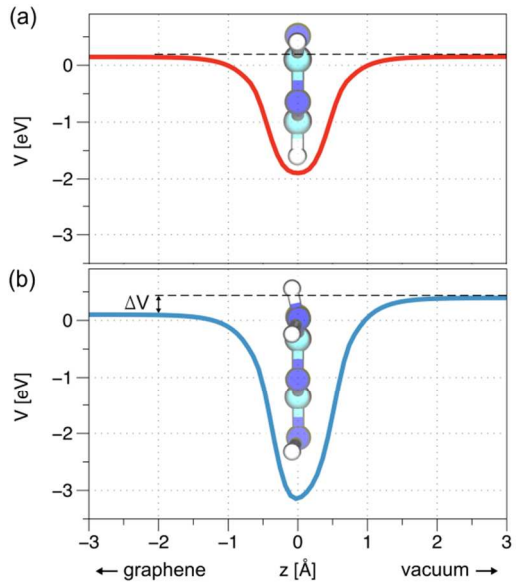

Fig 6. Plane averaged electrostatic potential of free (a) triazine and (b) melamine as a function of z using. The positions of atoms in the free molecules correspond to the adsorbed geometry of the molecules on graphene. ΔV indicates the energy difference between the vacuum levels oriented toward graphene and vacuum.

Conclusions

In conclusion, by employing a combination of electronic transport and XPS measurements, we have investigated the effects of physisorbed molecules on the graphene electronic structure and charge transfer mechanism. It has been found that triazine and melamine produce small and robust changes in the electronic properties of graphene, causing weak p-type doping of graphene, a reduction in graphene conductivity and a very strong coverage and molecular dipole moment dependence. These effects have a significant role on the observed electronic structure modification of graphene even at very small coverage of molecules, showing a great promise for sensing applications. The observed data have been explained by theoretical modelling using a simple electrostatic model and density functional theory calculations. Our results show that adsorbed molecules containing polar functional groups with strong electric dipole moments on graphene exhibit different coverage behaviour to nonpolar molecules. Layers of polar molecules on graphene demonstrate strong depolarization effects, which can results in moderate modifications of the electronic structure of graphene close to the Fermi level. These effects open up a wide range of opportunities for recognition of different molecules on graphene-based sensor devices.

Acknowledgements

This research was supported under Australian Research Council's Discovery Projects funding scheme (project number DE120101100) and by computational resources on the NCI National Facility through the National Computational Merit Allocation Scheme. The authors wish to acknowledge the facilities and the scientific assistance of the Soft X-ray beamline at the Australian Synchrotron, Victoria, Australia. M. K. acknowledges the support from by Czech Ministry of Education, Youth and Sports (ERC-CZ: LL1301).

Notes and references

[a] *School of Physics, The University of Melbourne, Victoria 3010, Australia; Email: jiri.cervenka@gmail.com*
[b] *Australian Synchrotron, 800 Clayton, Victoria 3168, Australia*
[c] *Department of Physics, La Trobe University, Victoria 3086, Australia*
[d] *School of Physics, Monash University, Victoria 3800, Australia*
[e] *Department of Materials Engineering, Monash University, Victoria 3800, Australia*
[f] *J. Heyrovsky Institute of Physical Chemistry of the ASCR, v. v. i., Prague, Czech Republic*

* *Corresponding author*
[#] *Current address: NanoGeoScience, Nano-Science Centre, University of Copenhagen, Universitetsparken 5, 2100 København Ø, Denmark*
[$] *Current address : Department of Chemistry, Center for Nanotechnology & Advanced Materials, Bar Ilan University, Ramat Gan 52900, Israel*

† Electronic Supplementary Information (ESI) available. See DOI: 10.1039/b000000x/

1. J. T.-W. Wang, J. M. Ball, E. M. Barea, A. Abate, J. A. Alexander-Webber, J. Huang, M. Saliba, I. Mora-Sero, J. Bisquert, H. J. Snaith, and R. J. Nicholas, *Nano Lett.*, 2014, **14**, 724–730.
2. S. Pang, Y. Hernandez, X. Feng, and K. Müllen, *Adv. Mater.*, 2011, **23**, 2779–2795.
3. W. Yuan and G. Shi, *J. Mater. Chem. A*, 2013, **1**, 10078.
4. S. Braun, W. R. Salaneck, and M. Fahlman, *Adv. Mater.*, 2009, **21**, 1450–1472.
5. H. Ishii, K. Sugiyama, E. Ito, and K. Seki, *Adv. Mater.*, 1999, 11, 605–625.
6. K. S. Novoselov, V. I. Fal'ko, L. Colombo, P. R. Gellert, M. G. Schwab, and K. Kim, *Nature*, 2012, **490**, 192–200.
7. P. L. Levesque, S. S. Sabri, C. M. Aguirre, J. Guillemette, M. Siaj, P. Desjardins, T. Szkopek, and R. Martel, *Nano Lett.*, 2011, **11**, 132–137.
8. K. S. Novoselov, *Science*, 2004, **306**, 666–669.
9. Y.-J. Yu, Y. Zhao, S. Ryu, L. E. Brus, K. S. Kim, and P. Kim, *Nano Lett.*, 2009, **9**, 3430–3434.
10. A. K. Singh, M. W. Iqbal, V. K. Singh, M. Z. Iqbal, J. H. Lee, S.-H. Chun, K. Shin, and J. Eom, *J. Mater. Chem.*, 2012, **22**, 15168.
11. J. Park, W. H. Lee, S. Huh, S. H. Sim, S. B. Kim, K. Cho, B. H. Hong, and K. S. Kim, *J. Phys. Chem. Lett.*, 2011, **2**, 841–845.
12. A. Tadich, M. T. Edmonds, L. Ley, F. Fromm, Y. Smets, Z. Mazej, J. Riley, C. I. Pakes, T. Seyller, and M. Wanke, *Appl. Phys. Lett.*, 2013, **102**, 241601.

13. F. Schedin, A. K. Geim, S. V. Morozov, E. W. Hill, P. Blake, M. I. Katsnelson, and K. S. Novoselov, *Nat. Mater.*, 2007, **6**, 652–655.
14. S. J. Park, O. S. Kwon, S. H. Lee, H. S. Song, T. H. Park, and J. Jang, *Nano Lett.*, 2012, **12**, 5082–5090.
15. S. Borini, R. White, D. Wei, M. Astley, S. Haque, E. Spigone, N. Harris, J. Kivioja, and T. Ryhänen, *ACS Nano*, 2013, **7**, 11166–11173.
16. G. Liu, S. Rumyantsev, M. S. Shur, and A. A. Balandin, *Appl. Phys. Lett.*, 2013, **102**, 093111.
17. T. O. Wehling, K. S. Novoselov, S. V. Morozov, E. E. Vdovin, M. I. Katsnelson, A. K. Geim, and A. I. Lichtenstein, *Nano Lett.*, 2008, **8**, 173–177.
18. L. H. Hess, M. Jansen, V. Maybeck, M. V. Hauf, M. Seifert, M. Stutzmann, I. D. Sharp, A. Offenhäusser, and J. A. Garrido, *Adv. Mater.*, 2011, **23**, 5045–5049.
19. A. Reina, H. Son, L. Jiao, B. Fan, M. S. Dresselhaus, Z. Liu, and J. Kong, *J. Phys. Chem. C*, 2008, **112**, 17741–17744.
20. M. Kalbac, O. Frank, and L. Kavan, *Carbon*, 2012, **50**, 3682–3687.
21. Y. Shi, X. Dong, P. Chen, J. Wang, and L.-J. Li, *Phys. Rev. B*, 2009, **79**, 115402.
22. P. C. Rusu, G. Giovannetti, C. Weijtens, R. Coehoorn, and G. Brocks, *J. Phys. Chem. C*, 2009, **113**, 9974–9977.
23. J. Martin, N. Akerman, G. Ulbricht, T. Lohmann, J. H. Smet, K. von Klitzing, and A. Yacoby, *Nat. Phys.*, 2008, **4**, 144–148.
24. S. Das Sarma and E. H. Hwang, *Phys. Rev. B*, 2013, **88**, 035439.
25. Q. Li, E. H. Hwang, E. Rossi, and S. Das Sarma, *Phys. Rev. Lett.*, 2011, **107**, 156601.
26. W. Gannett, W. Regan, K. Watanabe, T. Taniguchi, M. F. Crommie, and A. Zettl, *Appl. Phys. Lett.*, 2011, **98**, 242105.
27. C. R. Dean, A. F. Young, I. Meric, C. Lee, L. Wang, S. Sorgenfrei, K. Watanabe, T. Taniguchi, P. Kim, K. L. Shepard, and J. Hone, Nat. Nanotechnol., 2010, **5**, 722–726.
28. J.-H. Chen, C. Jang, S. Adam, M. S. Fuhrer, E. D. Williams, and M. Ishigami, *Nat. Phys.*, 2008, **4**, 377–381.
29. O. L. A. Monti, *J. Phys. Chem. Lett.*, 2012, **3**, 2342–2351.
30. S. H. Chou, J. Voss, I. Bargatin, A. Vojvodic, R. T. Howe, and F. Abild-Pedersen, *J. Phys. Condens. Matter*, 2012, **24**, 445007.
31. V. Vlahos, J. H. Booske, and D. Morgan, *Phys. Rev. B*, 2010, **81**, 054207.
32. A. Natan, Y. Zidon, Y. Shapira, and L. Kronik, *Phys. Rev. B*, 2006, **73**, 193310.
33. L. Romaner, G. Heimel, and E. Zojer, *Phys. Rev. B*, 2008, **77**, 045113.
34. K.-H. Jin, S.-M. Choi, and S.-H. Jhi, *Phys. Rev. B*, 2010, **82**, 033414.
35. X. Zhang, T. Chen, Q. Chen, L. Wang, and L.-J. Wan, *Phys. Chem. Chem. Phys.*, 2009, **11**, 7708.
36. A. J. Martínez-Galera and J. M. Gómez-Rodríguez, *J. Phys. Chem. C*, 2011, **115**, 23036–23042.
37. A. K. M. Newaz, Y. S. Puzyrev, B. Wang, S. T. Pantelides and K. I. Bolotin, *Nat. Commun.*, 2012, **3**, 734.
38. S. Wu, R. Yang, M. Cheng, W. Yang, G. Xie, P. Chen, D. Shi and G. Zhang, *Appl. Phys. Lett.*, 2014, **105**, 063113.
39. D. B. Farmer, R. Golizadeh-Mojarad, V. Perebeinos, Y.-M. Lin, G. S. Tulevski, J. C. Tsang and P. Avouris, Nano Lett., 2009, 9, 388–392.
40. B. Huard, N. Stander, J. Sulpizio and D. Goldhaber-Gordon, *Phys. Rev. B*, 2008, **78**, 121402(R).
41. J. Hölzl, F. K. Schulte, and H. Wagner, Eds., *Solid Surface Physics*, Springer-Verlag, Berlin/Heidelberg, 1979, vol. 85.
42. G. Kresse and J. Hafner, *VASP the Guide*, University of Vienna, 2007.
43. J. P. Perdew, K. Burke, and M. Ernzerhof, *Phys. Rev. Lett.*, 1996, **77**, 3865–3868.
44. S. Grimme, *J. Comput. Chem.*, 2006, **27**, 1787–1799.